Experimental study of the effect of the reduced frequency in the airfoil`s aerodynamic characteristics

J.A. Cárdenas Rondón*, M. Ogueta Gutiérrez** and S. Franchini Longhi***

*Instituto Universitario de Microgravedad "Ignacio Da Riva" (IDR/UPM)

Plaza del Cardenal Cisneros, 3, 28040 Madrid; ja.cardenas@alumnos.upm.es

**Instituto Universitario de Microgravedad "Ignacio Da Riva" (IDR/UPM)

Plaza del Cardenal Cisneros, 3, 28040 Madrid; mikel.ogueta@upm.es

*** Instituto Universitario de Microgravedad "Ignacio Da Riva" (IDR/UPM)

Plaza del Cardenal Cisneros, 3, 28040 Madrid; s.franchini@upm.es

Abstract

The aim of this research is to describe a dynamic system developed to analyse the characteristics of airfoils immersed in an unsteady flow, being able to reproduce different movement including coupled bending and torsion. Using an airfoil model with pressure taps, NACA 0015 was analysed in two cases: bending motion and flutter, both with a reduced frequency of 0.086. The hysteresis loops of both cases are presented. An outstanding different of c_l and c_d was observed depending on whether the effective angle of attack was increased or decreased. The need to create a catalogue of airfoils in unsteady regime is revealed.

1. Introduction

The studies about unsteady aerodynamics of airfoils present a considerable technical interest. The wide range of technical fields which are influenced by this discipline is the reason. As an example: the design of fixed wing airplanes, where the aeroelastic phenomenon of flutter requires the study of the hysteresis of the aerodynamic loads; the rotary wing aircrafts, where the change of pitch angle of the blades in order to maintain the equilibrium in roll, force to analyse the dynamic behaviour of the airfoil [1]; the study of the flight of insects, or more recently, the research about flapping wing aerodynamics as a possible propulsion and lift generation mechanism for micro air vehicles and nano air vehicles [2]. Another outstanding discipline influenced by unsteady aerodynamic is wind energy. The immense increase in the energy consumption, and the environmental demands, have led the industry to design ever increasing wind turbines, and blades with ever increasing aspect ratio. This is the reason why the aeroelastic phenomena takes a strong relevance. Hansen [3] and Young [4] have compiled the advances made in this topic.

In relation to wind turbines it is necessary to highlight, that at present the uncertainty in design calculations for performance predictions is around 10% to 20%, and the uncertainty in predictions of the aerodynamic load is around 30% [5]. The main reason of this uncertainty is the difficulty of correctly calculating and predicting of the aerodynamic loads in airfoils immersed in unsteady flows. This proves the need to continue the research on this subject. The origin of the unsteady behaviour in the performance of wind turbines are, mainly, in the environment in which they typically operate: on one hand they usually work immersed on the wake of other wind turbine, in the case of wind fields; and, on the other hand, wind turbines operate in the presence of the earth boundary layer, which is inherently turbulent. Holierhoek [5] has compiled and compared different methods for calculations of the dynamic stall, demonstrating the great difference between the predictions of each method.

The unsteady aerodynamics are characterised by the appearance of the hysteresis loops in the aerodynamic coefficients (lift, drag and moment). In the resent years a wide range of research are carried out in order to analyse these loops and to determine what parameters influence them. There are relevant parameters that influence them as: the free stream velocity; the position of the pitch axis; the mean angle in case of sinusoidally movement (or periodically in general); the amplitude and the phase between coupled movement and, the parameter that has been studied with most interest, the reduced frequency, k, defined as $k = \pi f c/u_\infty$, where f represents the frequency of the movement in Hz, c represents the chord of the airfoil in metres and u_∞ the free stream velocity. Sarkar and Venkatraman [6] studied the dynamic stall for high reduced frequency ($k > 1$) and mean angles between 25 and 45 degrees, with sinusoidally pitching

movement. Tsang [7] analysed the hysteresis loops of an airfoil NACA 0012, for reduced frequencies between 0.005 and 0.04, with a sinusoidal movement; and Parker [1] analysed an airfoil NACA 0012 oscillating near to the static stall angle and a reduced frequency up to 0.15. Even if the sinusoidally movement is the most studied, there are researches with different cinematic conditions, such as a constant rate pitching airfoil, NACA 0015 was analysed by Visbal [8]. The present study was carried out at "Instituto Universitario de Microgravedad Ignacio Da Riva" (IDR/UPM). It details the dynamic system, which was designed to analyse, experimentally, the aerodynamic behaviour of an airfoil with a coupled bending/torsion movement, as well as, a simple torsion movement or a simple bending movement. The dynamic system is based on a close loop control system, that is detailed in this study. The bending motion is produced by a triphasic motor, and the torsion movement is made by a stepper motor. Dynamic systems based on stepper motors are commonly used [1,2] for their precision and their ability to achieve complex movements. The main difference between the system detailed in this research and others stepper motor-based systems is the large size of the airfoils that allows testing, which allows testing airfoils with a high density of pressure taps.

This research exposes the results obtained after testing an NACA 0015 airfoil in bending motion, and in coupled motion (bending/torsion) with 90º phase. In both cases the reduced frequency was 0.06. The hysteresis loops of lift coefficient, c_l, and drag coefficient, c_d, and the distribution of pressure coefficient, c_p, around the surface of the airfoil are presented. The results are not only compared with the static case, but also with similar studies carried out in the same wind tunnel [9] in order to validate the current dynamic system.

2. Experimental set-up

2.1 Wind tunnel

This research was realized in the wind tunnel AB6, located in the facilities of IDR/UPM, on the Montegancedo campus. This is a subsonic open-return wind tunnel. Its geometrical characteristics guarantee the two-dimensional flow in the test area. The dimensions of its test section are: 0.5 m wide and 2.5 m high. This wind tunnel allows to test large size airfoils (300 mm of chord) with a high density of pressure taps. Additionally, the dimensions of the test camber avoid the need for solid blockage, wake blockage or streamline curvature corrections, even for large angles of attack [10]. In this wind tunnel, a maximum speed of 35 m/s can be reached in the test area, with a turbulence intensity lower than 2% [9].

2.2 Dynamic System

The dynamic system has been developed in the facilities of IDR/UPM. The development of this system responds to the continuation of a line of research dedicated to the study of airfoils of wind turbines and the analysis of their unsteady aerodynamic behaviour. Therefore, this dynamic system is based on a previous one, that can be found in [9].
This dynamic system was developed in order to achieve a coupled movement of bending and torsion, as well as movements with a single degree of freedom (torsion or bending).
The main characteristic of the mechanism is that it does not present mechanical restrictions and ligatures between the movements that are coupled. A closed loop control system is responsible for coupling both movements (bending and torsion) in real time, without the need of a mechanical connection between them. This has several advantages: mechanical elements that hinder the operation of the system are eliminated and the effective coupling between both movements can be ensured. It gives a wider range of parameters to be studied.

2.2.1 Hardware

The system consists mainly of two motors, one in charge of the movement of bending of the airfoil (bending motor) and the other one in charge of the movement of torsion (torsion motor). The bending motor is a three-phase motor of ABB (M2AA 132 3GAA132214-ASE) with an operational torque of 54.4 N·m. This motor, with a rod-crank system, moves a platform vertically. This platform supports the torsion motor and the airfoil. The torsion motor is a Nanotec stepper motor (ST11018L8004-B NEMA 42) with an operational torque of 13 N·m. It directly moves the airfoil shaft through a flexible single-disc coupler (MDS-63C-20-KT-25). The entire assembly is mounted on a side wall of the test area. Additionally, the rod-crank system has a counterweight to centre the load of the motor of bending. Both motors have attached digital incremental encoders, which measure the position of the shaft of each motor. The encoder attached to the motor of bending is a 1024 ppr (pulse per revolution) encoder from Kubler (8.KIS40.1342.1024). This encoder is coupled to the shaft of the motor by a double loop coupling (DKPS 291804/10). The shaft of the motor of torsion is connected to a 1000 ppr encoder of Nanotec (NOE2-05-B06). In addition, there is an optical sensor (opb620) in order

to count each revolution of the motor of bending and correct possible errors of the encoders. Finally, the stepper motor is controlled by the Geckodrive G201X driver, which controls the motor with a constant micro stepping of 0.18º per pulse. This driver has a fan to prevent overheating.

The rod-crank system consists of a fixed-length rod connected to a crank with two possible connection points. With this, two different strokes of the bending movement can be achieved: $0.125c$ (38 mm) and $0.25c$ (75 mm). In relation to the movement of torsion, the stepper motor was chosen to be able to produce a sinusoidal movement of 30º of semi amplitude and 1 Hz of frequency, with a mean angle of attack of 10º and a free stream velocity of 15 m/s.

The figure 1 shows the dynamic system and the main components.
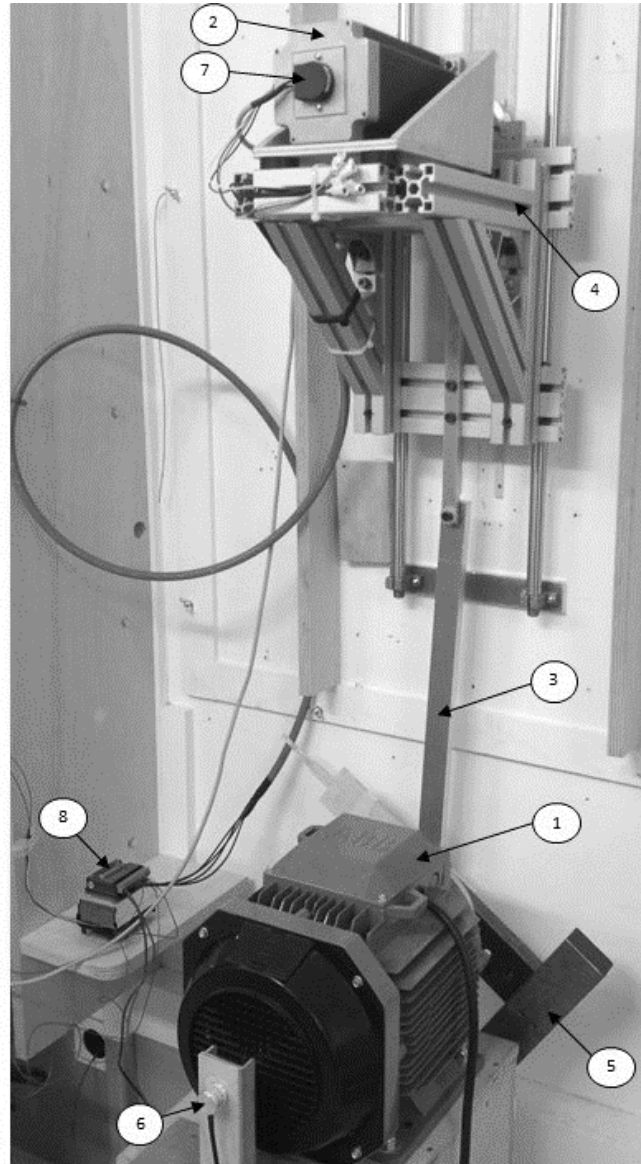
Figure 1: Dynamic system. 1: motor of bending; 2: motor of torsion; 3: rod-crank system; 4: platform which support the motor of torsion an the airfoil; 5: counterweight; 6: 1024 ppr encoder; 7: 1000 ppr encoder; 8: driver of the stepper motor with fan.

2.2.1 Software

All the electronics elements of the dynamic system are connected to a PC using the DAQ device NI PC 6220 and NI 6034E of National Instruments. The electronics elements are connected to the DAQ devices through the modules NISCB-68 and NI CB-68LP or National Instruments. The connection scheme is represented in the Figure 2.
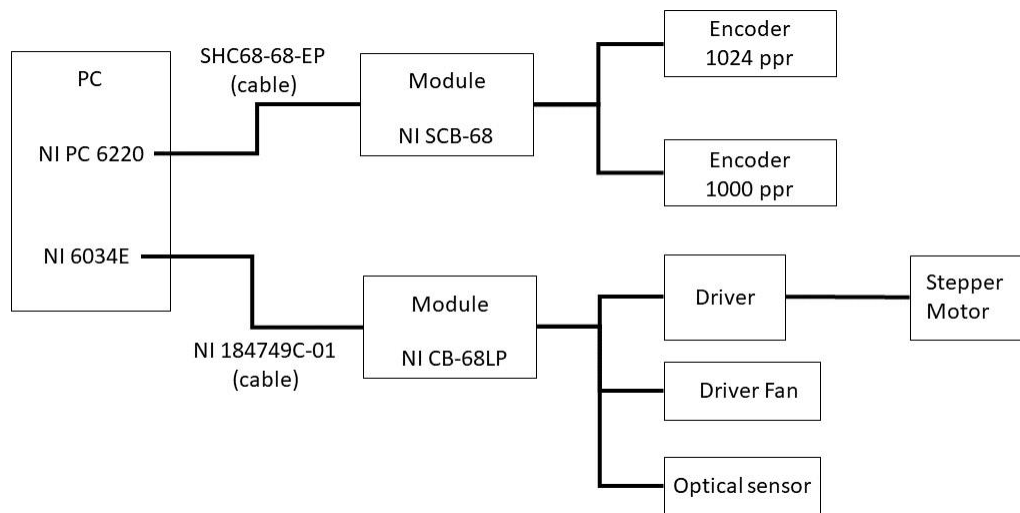
Cárdenas, J.A., M. Ogueta, S. Franchini

Figure 2: Connection scheme of the electronic elements.

In order to create the coupled motion and ensure the correct function during the test, a closed loop control system was developed using the software of Labview of National Instrument. Figure 3 shows the scheme of the close loop control system. In every instant of the movement, the shaft of the bending motor will have a certain angle, Υ, which is defined as $\Upsilon = \omega_b t$, where ω_b is the angular speed of the bending motor in rad/s and t is the time of the certain instant. The encoder attached to the bending motor shaft will measure this angle. Then, using a cinematic relationship, the angle of torsion, Θ_t, that the airfoil should have at this position of bending, is calculated.

Also, the real angle of torsion, Θ_r, (the angle of torsion that has the airfoil actually) is measured using the encoder attached to the motor of torsion. After that, an error, e , is calculated as $e = \Theta_t - \Theta_r$. In order to generate the control signal, the error is divided by the angle per pulse of the stepper motor, in these case $0.18°$ per pulse, and rounding to the nearest integer, the number of pulse of the stepper motor to reach the target angle is obtained. The number of pulses is sent to the driver to move the stepper motor. Additionally, the vertical displacement of the airfoil is calculated using the angle of the bending motor, Υ, and the ligatures of the rod-crank system.

Figure 4 shows an example of coupled motion performed with this dynamic system in which both movements, bending and torsion, are sinusoidal, and the torsion movement has a phase of 90º respect de movement of bending; the movement is represented versus the non-dimensional time, τ, defined as $\tau = t/T$, where T is the period of the movement.
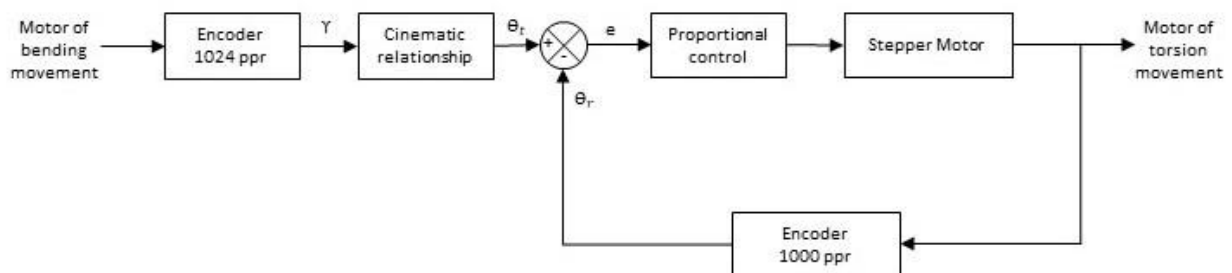

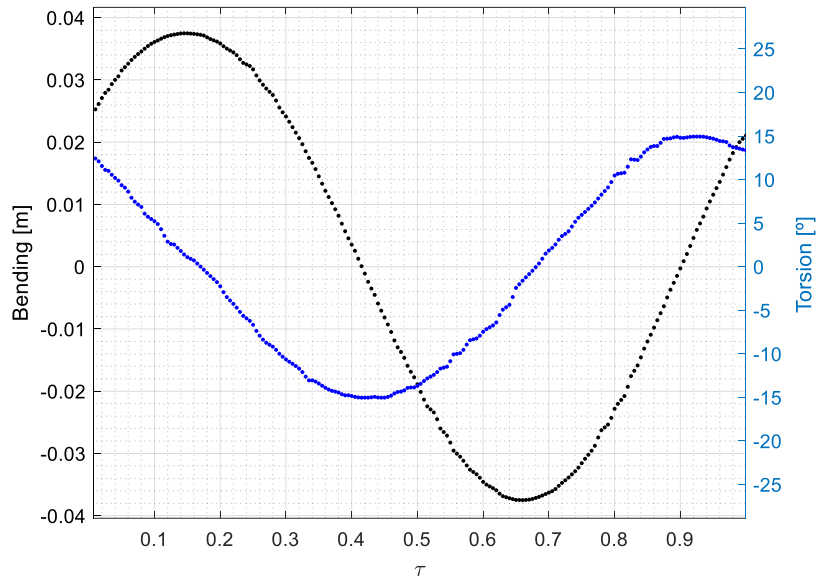Figure 3: Scheme of the closed loop control system.

Figure 4: Phase-averaged coupled movement represented versus the non-dimensional time, τ.

2.3 Airfoil

The symmetric airfoil NACA 0015 was the analysed in this study. The model used has a 300 mm chord and the pitch axis is located at ¼ of the chord. To measure the aerodynamic loads, 61 pressure taps are used. Figure 5 shows the position of each pressure tap. They are numbered starting at the trailing edge of the upper surface in an anti-clockwise direction and ending at the trailing edge of the lower surface. The distribution of pressure taps is not uniform around the chord, being higher in the leading edge and lower in the trailing edge. Due to geometrical characteristics, the taps closest to the trailing edge are located at 90% of the chord. The model has a wingspan of 49 cm covering the test area side by side once installed. The number of taps was selected according to the pressure scanner used. To measure the pressure a ZOC-33/64PxX2 of Scanicalve Corp is used. That pressure scanner can measure 64 taps simultaneously per sample.
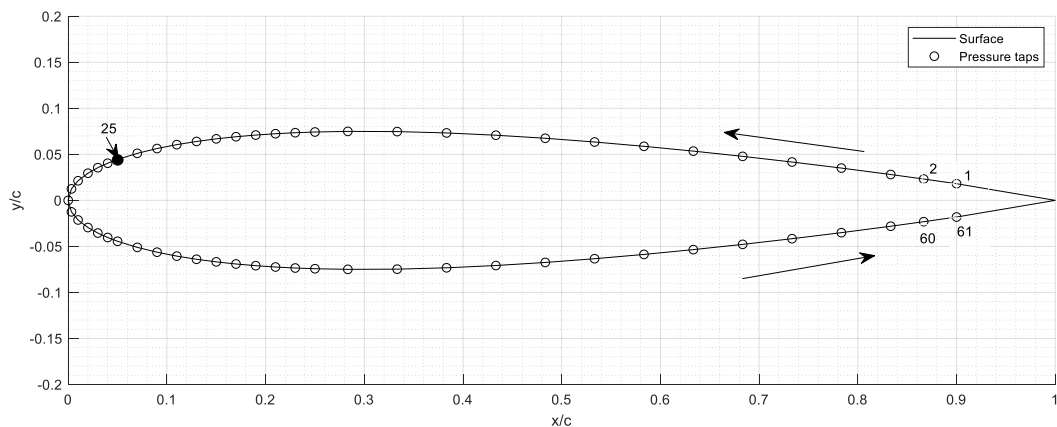

Figure 5: Position and numbering of the pressure taps of the airfoil tested. Highlighted tap 25, that is analysed later.

3. Formulation

3.1 Non-dimensional coefficients

In this study different aerodynamic non-dimensional coefficient are analysed and presented. With the differential pressure measured, the pressure coefficient can be calculated as:

$$c_p = \frac{p - p_\infty}{\frac{1}{2}\rho u_\infty{}^2} \tag{1}$$

where p is the static pressure of the point where the coefficient is calculated and p_∞ is the static pressure of the free stream.

With the values of the pressure coefficients, the rest of the coefficients can also be calculated. These coefficients are the drag, c_d, lift, c_l, and moment coefficient, c_m, and they are defined as:

$$c_l = \frac{l}{\frac{1}{2}\rho u_\infty{}^2 c} \tag{2}$$

$$c_d = \frac{d}{\frac{1}{2}\rho u_\infty{}^2 c} \tag{3}$$

$$c_m = \frac{m}{\frac{1}{2}\rho u_\infty{}^2 c^2} \tag{3}$$

where l is the lift per wingspan unit; ρ is the density of the air; u_∞ is the free stream velocity; c is the chord of the airfoil; d is the aerodynamic drag per wingspan unit and m the aerodynamic moment per unit of wingspan.

4. Results

4.1 Movement of bending

In this case, the airfoil NACA 0015 was tested with a sinusoidal bending movement. The vertical position of the airfoil, $h(t)$, follows the expression:

$$h(t) = A_h \sin(2\pi f t) \tag{5}$$

where A_h represents the amplitude of the movement in metres; t represents the time in seconds and f represents the frequency of the movement in Hz. The airfoil was tested with an amplitude, A_h, of $0.125c$ (38 mm) and with a frequency, f, of 1 Hz. The free stream velocity in the test area, u_∞, was, approximately, 11 m/s. The angle of torsion, θ_0, is constant an equal to 9°. In these conditions, the reduced frequency, k, was 0.086.

To represent and analyse the results an effective angle of attack, α_{ef}, was calculated as follows [11]:

$$\alpha_{ef}(t) = \theta - \tan^{-1}\left(\frac{\dot{h}}{u_\infty}\right) \tag{6}$$

where $\dot{h}$ is the vertical velocity $\left(\dot{h} = {dh}/{dt}\right)$. The figure 6 shows the phase-averaged effective angle of attack and the vertical velocity versus the non-dimensional time, τ.
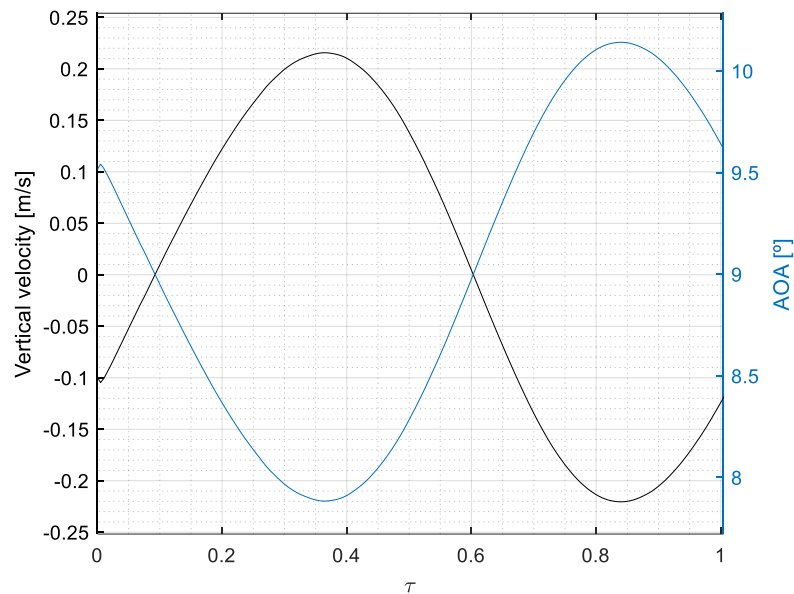
Figure 6: Phase-averaged effective angle of attack and vertical velocity versus non-dimensional time.

Figure 7 shows the hysteresis loop of the lift coefficient obtained under the conditions described before and the directions of this loop. As shown in the figure, the lift coefficient is significantly different if the airfoil is increasing the angle of attack or decreasing it. This difference decreases if the airfoil is moving around the maximum or minimum effective angle of attack. On the contrary, it is maximum near to the balance angle, reaching differences of up to 10%. If the airfoil is increasing the effective angle of attack, the lift coefficient is higher than if the airfoil is decreasing it.
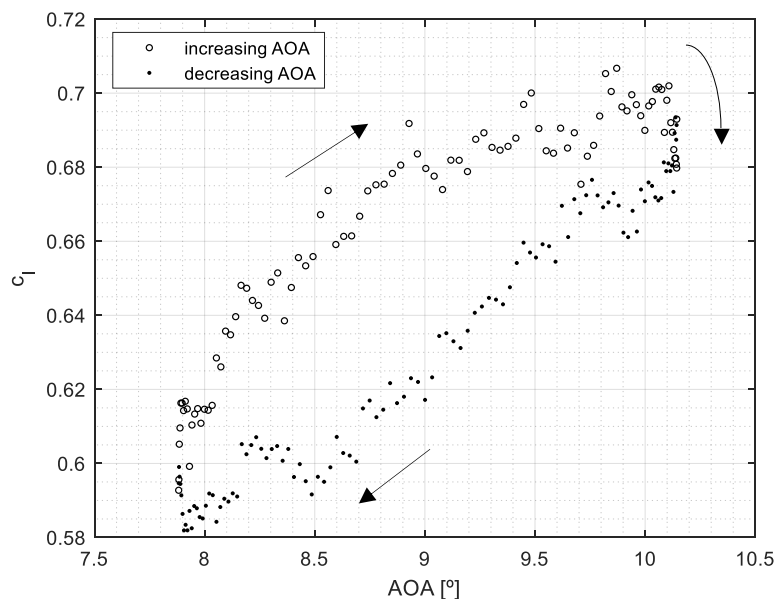

Figure 7: Hysteresis loop of the lift coefficient versus the effective angle of attack in a bending motion. The direction of the cycle is represented.

It was observed that, the variation in the lift coefficient may be related to an increase in the suction of the upper surface near to the leading edge when the airfoil increments the effective angle of attack. An increment of the effective angle of attack means, in a simple bending motion, that the airfoil is descending, as the figure 6 shows. In the figure 8 the phase-averaged coefficient of pressure distribution, along the chord for an effective angle of attack of 9º, is represented. It may be noted that the biggest difference between the distributions happens in the upper surface near to the leading edge. Additionally, the evolution in the coefficient of pressure of the pressure tap number 25 located in the upper surface, whose position is shown in figure 5, versus the angle of attack is represented in the figure 9. It shows that the pressure coefficient is lower for any angle of attack if it is increasing compared with the same angle if it is decreasing.
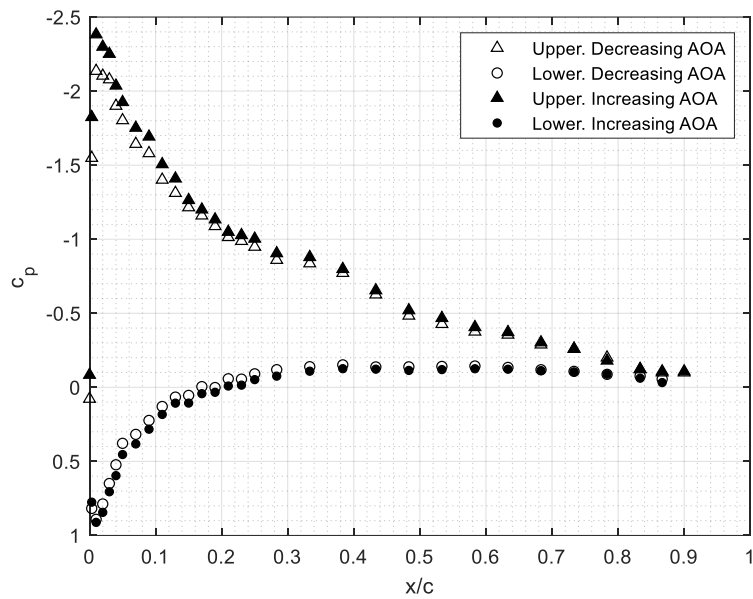
Figure 8: Phase-averaged coefficient of pressure distribution along the chord for an effective angle of attack of 9º in a bending motion.
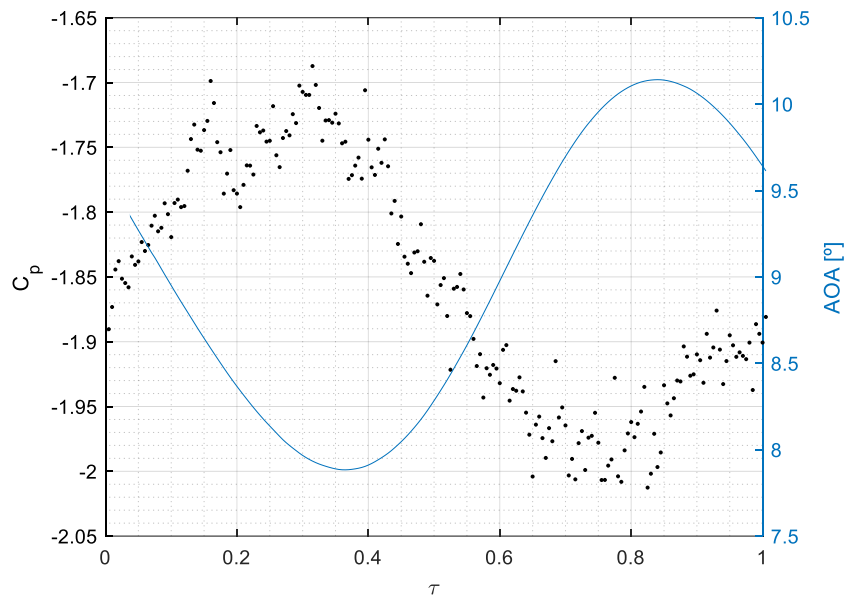
Figure 9: Phase-averaged coefficient of pressure in pressure tap number 25 versus the non-dimensional time in a bending motion. The effective angle of attack is also represented.

The drag coefficient was also calculated, and it is represented versus the lift coefficient in figure 10. In this case, the drag coefficient increases if the lift coefficient is incremented, however, the drag does not return by the same path if the lift coefficient is decreasing, being bigger in this case.
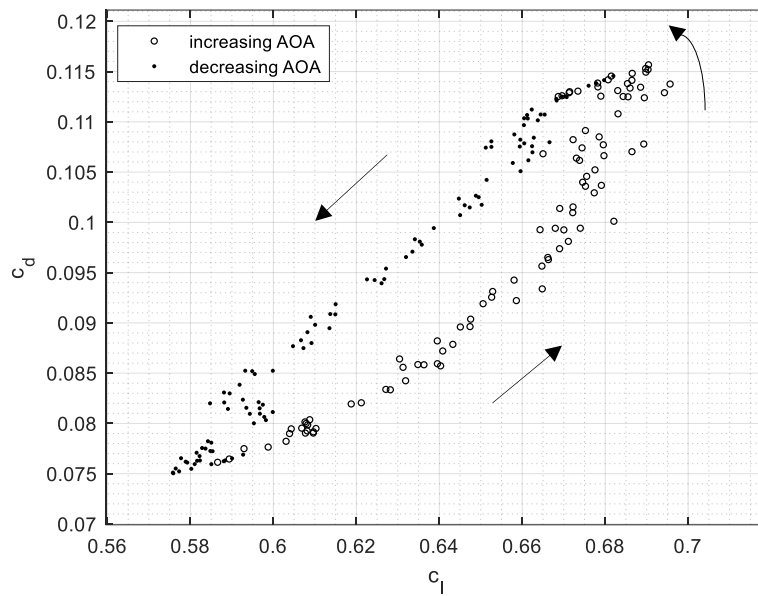
Figure 10: A polar of NACA 0015 oscillating in a bending motion between 7º and 11º. The direction of the cycle is represented.

4.2 Movement of coupled bending/torsion

In this case, the airfoil NACA 0015 was tested with a sinusoidal bending movement coupled with a sinusoidal torsion movement. The bending movement corresponds to the equation 5, and the torsion movement follows the expression:

$$\theta(t) = \theta_0 + A_\theta \sin(2\pi f t + \varphi) \tag{7}$$

being θ_0 the balance angle of torsion in radians; A_θ the amplitude of the torsion motion in radians; f the frequency of both movements (torsion and bending) and φ the phase between the torsion and bending. The airfoil was tested with an amplitude of the bending motion, A_h, of $0.125c$ (38 mm); an amplitude of torsion motion, A_θ, of 15º; with a phase, φ, of 90º; and with a frequency, f, of 1 Hz. The balance angle of torsion, θ_0, was 0º. The free stream velocity in the test area was, approximately, 11 m/s. In these conditions, the reduced frequency, k, was 0.086.
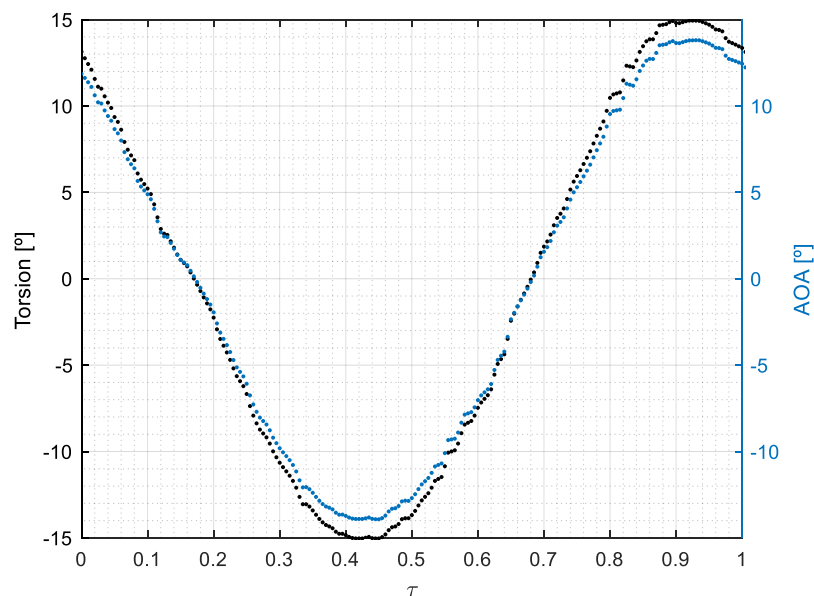

Figure 11: The phase-averaged effective angle of attack of the couple motion (blue) compared with the torsion angle (black) versus the non-dimensional time.

9

Analogous to the case of pure bending, the effective angle of attack was calculated using the expression 6. Figure 11 shows the effective angle of attack with regards to the non-dimensional time. As seen in the figure, the angle of attack and the torsion angle are in phase sinusoidal movements, being the maximum angle of attack (14º) lower than the maximum torsion angle (15º). This is due to the contribution of the bending movement.

The hysteresis loop of the lift coefficient, c_l, was calculated and it is shown in figure 12. From this figure some aspects were observed: the dynamic stall was not reached in this condition of movement and c_m presents a hysteresis loop with a small difference between increasing or decreasing the angle of attack. Also, it was observed that between -6º and 0º even being the angle of attack negative, when the airfoil is increasing the angle of attack it has a positive lift. And, analogously, between 0º and 7º, when the airfoil is decreasing the angle of attack the lift is negative. This happens in both cases near to the end of the bending stroke, where the acceleration of the bending motion is near to the maximum, and the acceleration of the torsion motion is near to the minimum.

Figure 13 shows the pressure coefficient of the pressure tap number 25 placed on the upper surface, whose position is depicted in figure 5. As shown in the figure, when the airfoil is decreasing the effective angle of attack between 0º and 7º, the pressure coefficient is positive. And, analogously, when the airfoil is increasing the angle of attack, between -10º and 0º the pressure coefficient is negative. This behaviour is opposite to the static case, in which a positive angle of attack supposes a negative coefficient pressure in the upper surface near to the trailing edge and a negative angle suppose a positive coefficient pressure.

The pressure coefficient distribution along the chord for an angle of attack of 5º is shown in figure 14. As seen in the figure, the distribution of pressure when the airfoil is increasing the effective angle of attack is noticeably different from the case in which the angle of attack is decreasing. It should be noted, that when the angle is decreasing, the upper surface has overpressure and the lower surface has suction, which is opposite to the static case.
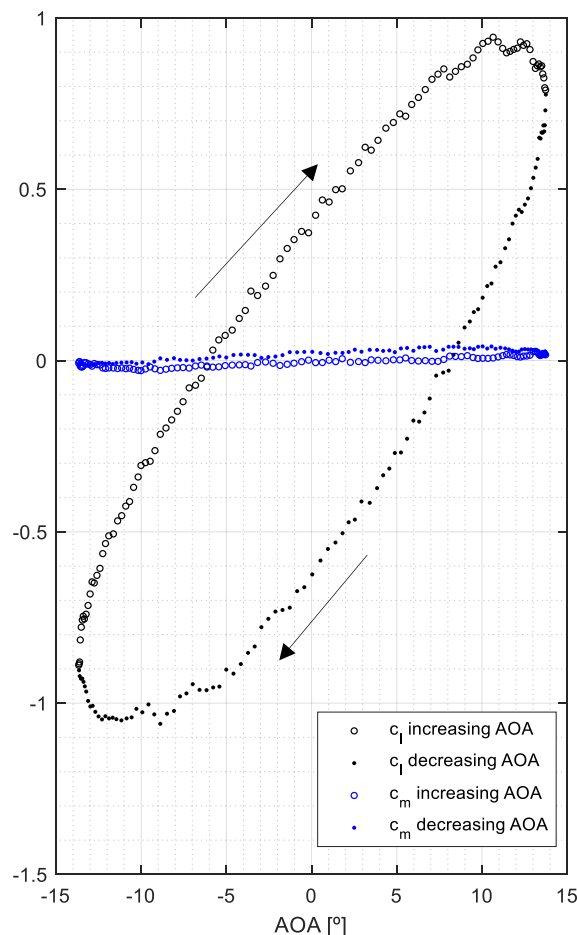

Figure 12: Hysteresis loops of c_l and c_m of NACA 0015 with coupled motion. The direction of the lift cycle is represented.
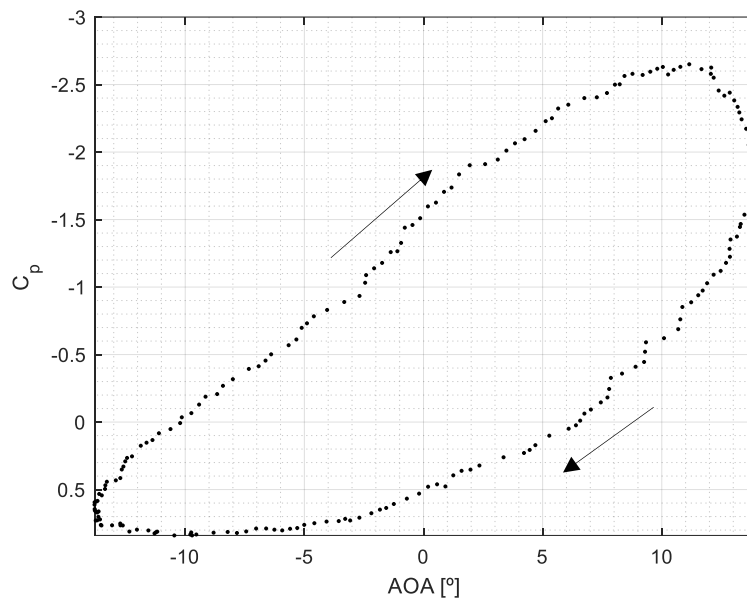
Figure 13: Phase-averaged evolution in the pressure coefficient of the pressure tap number 25 with regards to the angle of attack. The direction of the cycle is represented.
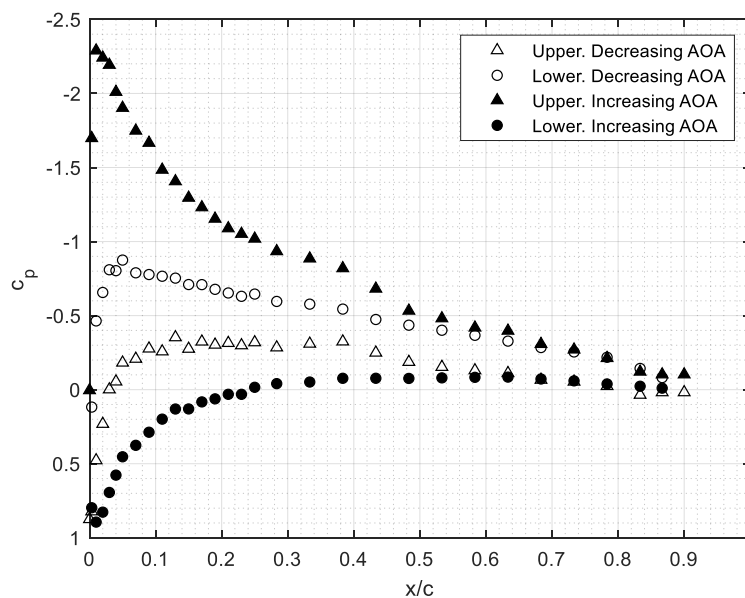

Figure 14: Pressure coefficient distribution along the chord for an effective angle of attack of 5°.

Additionally, the distribution of pressure coefficient along the cord of the static case was compared with the dynamic case. The figure 15 shows a comparison between the pressure distribution for an angle of 0° in the static case and the dynamic case corresponding to an increase of the effective angle of attack. In the static case both upper surface and lower surface has a similar distribution of pressure; which is consistent since it is a symmetric airfoil. On the contrary, in the dynamic case the pressure distribution is more similar to the case of an airfoil with positive camber.

Finally, the hysteresis loop of the drag coefficient was analysed and the polar of this coupled movement is presented in figure 16. As seen in the figure, in the polar, there are regions in which the c_d is negative. This does not have to mean really that the resistance can become negative in these angles, because in this study was analysed only the effect of pressure and it was not analysed the contribution of the viscosity. If all the contributions are to be taken into account, the determination of the drag force must be measured with load cells or a rack of pressure taps downstream should be placed in order to measure the full drag by measuring the wake pressure and the momentum method [12,13].

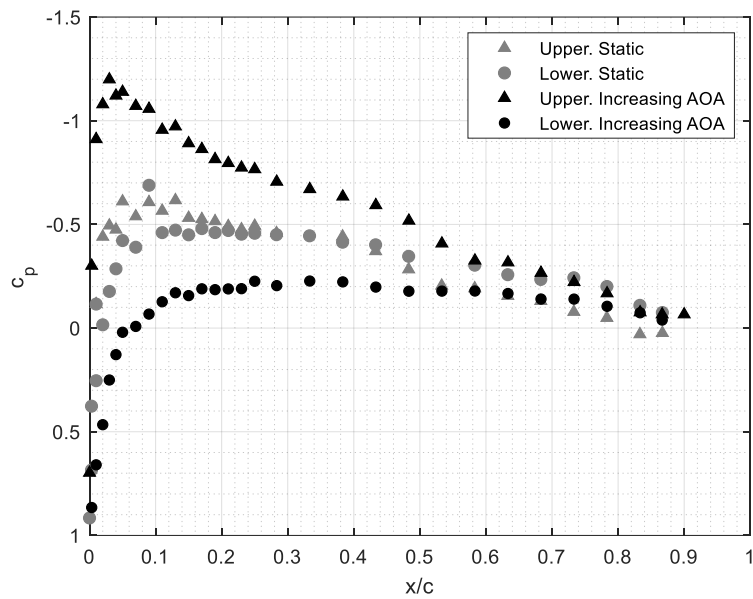Cárdenas, J.A., M. Ogueta, S. Franchini

Figure 15: Comparison between the pressure coefficient distribution along the chord in a static case and the dynamic case.
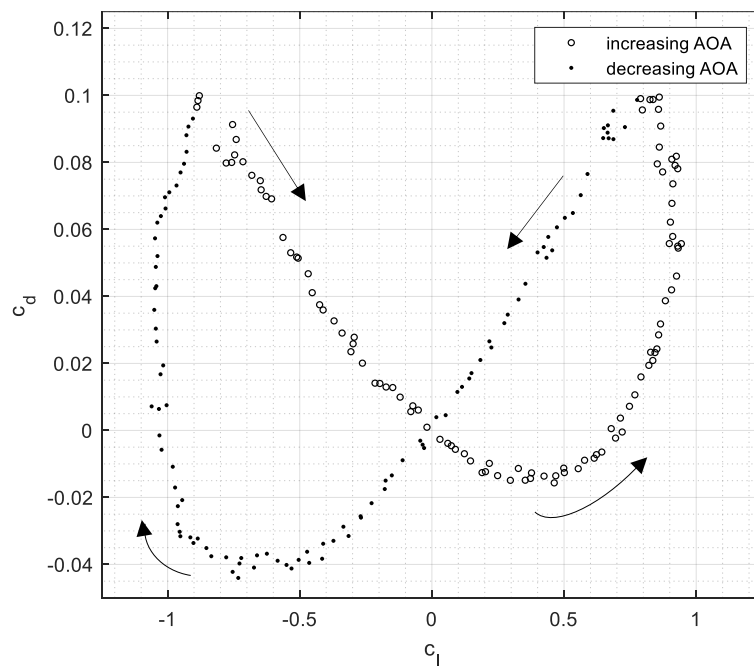

Figure 16: A polar of NACA 0015 in a coupled motion. The direction of the cycle is represented.

Additionally, the hysteresis loop of the lift coefficient was compared with the results obtained by Ibarra [9] testing the same airfoil under the same movement but with a different reduced frequency ($k = 0.063$) This comparation is shown in figure 17. It shows how increasing the reduced frequency also increases the area enclosed by the hysteresis curve. The difference between the lift coefficient to increase or decrease the angle of attack becomes more acute. However, the direction of the loop remains constant.
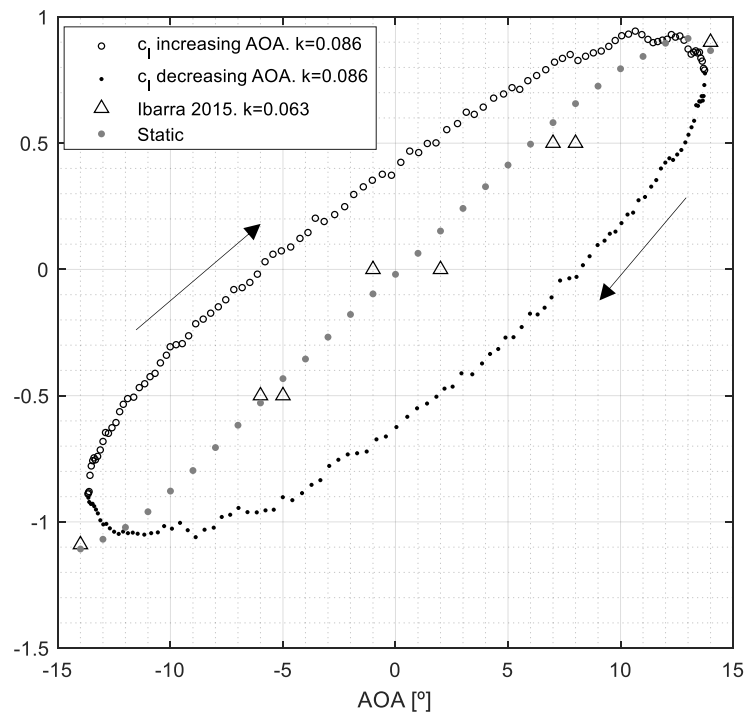
Figure 17: Comparison between the hysteresis loop of the lift coefficient ($k = 0.086$) and the results obtained by Ibarra [9] ($k = 0.063$). Static results are also depicted.

5. Conclusions

The results presented herein lead to several conclusions. The hysteresis loops of the aerodynamic coefficients, c_l and c_d, are extremely dependent of the movement that the airfoil follows; presenting different values of these coefficient for the same effective angles of attack if the airfoil follows a bending motion or a coupled bending/torsion movement. However, in both movements, bending and coupled, c_l is noticeably different if the effective angle of attack is increased or decreased, being greater, for the same angle of attack, in the case of increase of the effective angle of attack than in the decrease. Also, this variation of c_l is greater near to the balance affective angle of attack, in both movements. In the bending motion, this variation of c_l could be related with an increment in the suction of the trailing edge. In coupled bending/torsion movement there are some effective angles of attack [-6º to 0º] that even with a negative values, a positive lift can be produced and vice versa with some positive effective angles of attack [0º to 7º], because, for these effective angles of attack, the distribution of pressures along de chord on the upper surface ant the lower surface is inverse to the static case. Additionally, it was observed that an increase of the reduced frequency supposes, for the same movement, a notorious variation in the hysteresis loops.

These behaviours and this variability of the hysteresis cycles highlight the need to carry out an extensive testing campaign that analyses not only a large number of movements but also different airfoils, with the aim of creating a catalogue that helps the most accurate calculation of unsteady aerodynamic forces.

References

[1] Parker, A.G. 1976. Force and Pressure Measurements on an Airfoil Oscillating through Stall. J.Aircraft Vol 13, NO, 10: 823-827.

[2] Baik, Y.S., ang L.P. Bernal. 2012. Experimental study of pitching and plunging airfoils at low Reynolds numbers. Exp Fluids 53:1979-1992.

[3] Hansen, M.O.L., J.N. Sorensen, S. Voutsinas, N. Sorensen, H.Aa. Madsen. 2006. State of the art in wind turbine aerodynamics and aeroelasticity. Progress in Aerospace Sciences 42: 285-330.

[4] Young, J., J.C.S. Lai, and M.F. Platzer. 2014. A review of progress and challenges in flapping foil power generation. Progress in Aeroespace Science 67: 2-28.

[5] Holierhoek, J.G., J.B. de Vall, A.H. van Zuijlen, and H. Bijl. 2013. Comparing different dynamic stall models. Research article. Wind Energ. 16:139-158.

[6] Sarkar, S., and Venkatraman, K. 2006. Influence of pitching angle of incidence on the dynamic stall behaviour of a symmetric airfoil. European Journal of Mechanics B/Fluids 27 (2008) 219-238.

[7] Tsang, K.K.Y., So, R.M., and Wang X.Q. 2006. Dynamic stall behaviour from unsteady force measurements. Journal of Fluids and Structures 24 (2008) 129-150.

[8] Visbal, M.R. 1990. Dynamic Stall of a Constant-Rate Pitching Airfoil. J. Aircraft Vol. 27, NO,5.

[9] Ibarra, A.D. 2015. Aerodinámica no estacionaria en perfiles de aerogeneradores. PhD Thesis. Universidad Politécnica de Madrid, Escuela Técnica Superior de Ingenieros Aeronáuticos.

[10] Barlow, J.B., Rae, Jr, W.H., and Pope, A.1999. Low-Speed wind tunnel testing. Third edition. John Wiley & sons, INC. Third edition. Chapter 9.

[11] Kinsey, T. and Dumas, G. 2008. Parametric study of an oscillating airfoil in a power-extraction regime. AIAA J.,46(6), 1318-1330.

[12] Betz, A. 1925. A method for the direct determination of wing-section drag. National Advisory Committee for Aeronautics. Technical Memorandum No 337.

[13] Goett, H.J. 1988. Experimental Investigation of the Momentum Method for Determining Profile Drag. Report No. 660.